

# Electric-field control of spin waves at room temperature in multiferroic BiFeO<sub>3</sub>

P. Rovillain<sup>1</sup>, R. de Sousa<sup>2</sup>, Y. Gallais<sup>1</sup>, A. Sacuto<sup>1</sup>, M. A. Méasson<sup>1</sup>, D. Colson<sup>3</sup>, A. Forget<sup>3</sup>, M. Bibes<sup>4,5</sup>, A. Barthélémy<sup>4,5</sup> and M. Cazayous<sup>1\*</sup>

**To face the challenges lying beyond present technologies based on complementary metal-oxide-semiconductors, new paradigms for information processing are required. Magnonics<sup>1</sup> proposes to use spin waves to carry and process information, in analogy with photonics that relies on light waves, with several advantageous features such as potential operation in the terahertz range and excellent coupling to spintronics<sup>2</sup>. Several magnonic analog and digital logic devices<sup>3</sup> have been proposed, and some demonstrated<sup>4</sup>. Just as for spintronics, a key issue for magnonics is the large power required to control/write information (conventionally achieved through magnetic fields applied by strip lines, or by spin transfer from large spin-polarized currents). Here we show that in BiFeO<sub>3</sub>, a room-temperature magnetoelectric material<sup>5</sup>, the spin-wave frequency (>600 GHz) can be tuned electrically by over 30%, in a non-volatile way and with virtually no power dissipation. Theoretical calculations indicate that this effect originates from a linear magnetoelectric effect related to spin-orbit coupling induced by the applied electric field. We argue that these properties make BiFeO<sub>3</sub> a promising medium for spin-wave generation, conversion and control in future magnonics architectures.**

Magnetoelectric multiferroics possess coexisting magnetic and ferroelectric phases, with cross-correlation effects between magnetic and electric degrees of freedom<sup>6</sup>. As such, they can potentially be used to control spin-based properties by electric fields<sup>7</sup>, with very low associated power dissipation. This feature seems promising not only for spintronics, in which information is encoded by the spin polarization of the electrical current<sup>8</sup>, but also for magnonics that use magnetic excitations (spin waves) for information processing<sup>1</sup>. Indeed, just as coupling between magnetic and ferroelectric order parameters exists in multiferroics, coupled spin and lattice excitations termed electromagnons have also been demonstrated<sup>9</sup>. Such mixed excitations exist at low temperature in multiferroic manganites<sup>9</sup> and are suspected at room temperature in BiFeO<sub>3</sub> (ref. 10). Although in the former systems, electromagnons have been shown to depend on magnetic fields<sup>11</sup>, their predicted sensitivity to electric fields, at the heart of their potential applicative interest, remains to be demonstrated.

Here, we focus on BiFeO<sub>3</sub> (BFO), a special case among multiferroic materials. Indeed, BFO has a very high ferroelectric polarization reaching 100  $\mu\text{C cm}^{-2}$  (ref. 12) below  $T_C = 1,143$  K and becomes an antiferromagnet below  $T_N = 643$  K. The spins form a cycloid structure with a wavelength of  $\lambda_0 = 62$  nm and an

associated cycloid wave vector equal to  $Q = 2\pi/\lambda_0$  (refs 13–15). The magnetic cycloid lies in the  $(\bar{1}\bar{2}\bar{1})$  plane, formed by the ferroelectric polarization  $\mathbf{P}_1 \parallel [111]$  and the cycloid wave vector  $\mathbf{Q} \parallel [10\bar{1}]$  (Fig. 1a). An electric field can simultaneously induce the flop of the polarization and the cycloidal plane<sup>16</sup>. The electrical switch of antiferromagnetic–ferroelectric domains in BFO has been observed<sup>17,18</sup> and controlled in a ferromagnet–multiferroic heterostructure<sup>7</sup>. Here we report direct electric-field control of spin-wave states in BFO at room temperature.

In BFO, inelastic light scattering reveals two species of spin-wave excitation modes. These are observed in Raman spectra as two series of sharp peaks labelled cyclon ( $\phi_n$ ) and extra-cyclon modes ( $\psi_n$ ) below 70  $\text{cm}^{-1}$ , the frequency of the lowest phonon mode<sup>10,19,20</sup>. The cyclon  $\phi_n$  and extra-cyclon  $\psi_n$  modes correspond respectively to the spin oscillations in and out of the cycloidal plane (Fig. 1a) and their Raman scattering signatures are reported in Fig. 1c. These two species of magnons originate from the translational symmetry breaking<sup>21</sup> of the cycloidal ground state. The spin-wave momentum is no more conserved, and can be increased or decreased by a multiple of the cycloid wave vector  $Q$ . This leads to magnon zone folding at the Brillouin zone centre, where  $\phi_n$  and  $\psi_n$  correspond to magnon wave vectors equal to  $\mathbf{k} = n\mathbf{Q}$ .

The experimental set-up used to apply an electric field and to detect the optical excitations of spin waves is presented in Fig. 1b. The device consists of bottom and top (transparent) electrodes that enable the application of an electric field along the  $[010]$  and  $[0\bar{1}0]$  directions of a bulk BFO sample. The effect of the external electric field on the spin-wave modes is tracked in Fig. 1c. An external electric field applied along the  $[010]$  direction induces a blueshift of the  $\psi_n$  modes ( $\psi_2$  and  $\psi_3$ ) and a redshift of the  $\phi_n$  modes ( $\phi_2$ ,  $\phi_3$  and  $\phi_4$ ). The promise of this electric-field control depends on our ability to selectively tune the spin-wave states using the polarization hysteresis cycle and the switching of the polarization vector  $\mathbf{P}$ .

Figure 2a,b shows the frequency shift of the  $\phi_2$  (cyclon) and  $\psi_2$  (extra-cyclon) modes as a function of the polarization cycle. This figure demonstrates that the spin-wave modes are directly connected to the polarization hysteresis loop shown in Fig. 2c. With an initial polarization state  $\mathbf{P}_1 \parallel [111]$ , decreasing the applied electric field ( $E \parallel [010]$ ) induces an increase of the  $\phi_2$  mode frequency (red diamond, Fig. 2a) following path 1 in the polarization cycle. Travelling along path 2 with a negative electric field ( $E \parallel [0\bar{1}0]$ ), the frequency of the  $\phi_2$  mode (blue star) increases up to the flip of  $\mathbf{P}$  along the  $[1\bar{1}\bar{1}]$  direction ( $\mathbf{P}_2$ ) at critical electric field  $E_c \approx -35 \text{ kV cm}^{-1}$  (ref. 12). Beyond  $E_c$ , the frequency of  $\phi_2$  decreases. The hysteresis cycle can be completed along paths

<sup>1</sup>Laboratoire Matériaux et Phénomènes Quantiques (UMR 7162 CNRS), Université Paris Diderot-Paris 7, 75205 Paris cedex 13, France, <sup>2</sup>Department of Physics and Astronomy, University of Victoria, Victoria, British Columbia, V8W 3P6, Canada, <sup>3</sup>Service de Physique de l'Etat Condensé, CEA Saclay, IRAMIS, SPEC (CNRS URA 2464), F-91191 Gif sur Yvette, France, <sup>4</sup>Unité Mixte de Physique CNRS/Thales, 1 av. A. Fresnel, Campus de l'Ecole Polytechnique, F-91767 Palaiseau, France, <sup>5</sup>Université Paris-Sud, 91405 Orsay, France. \*e-mail: maximilien.cazayous@univ-paris-diderot.fr.

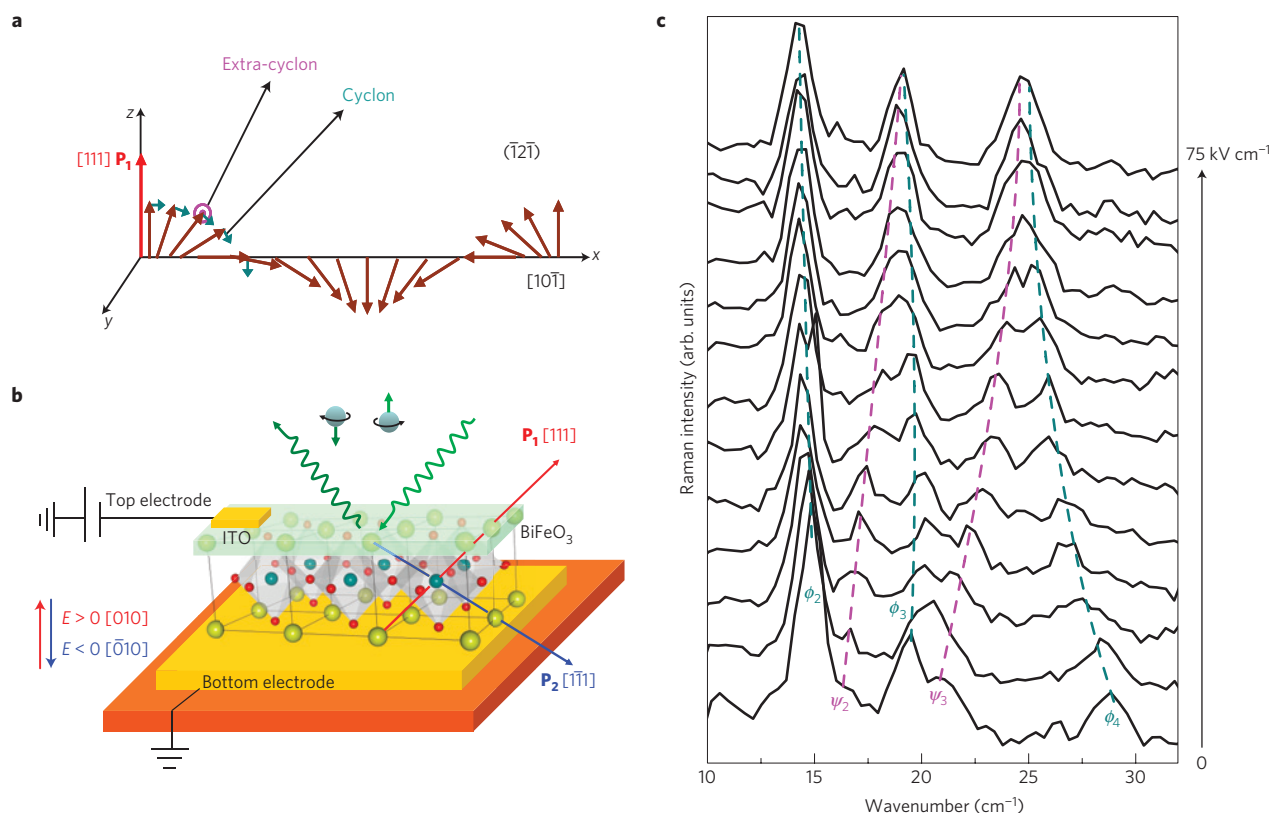


**Figure 1 | Electrical control of spin waves.** **a**, The spin cycloid ground state along with its low-energy excitations when the ferroelectric polarization  $\mathbf{P}_1$  points along the  $[111]$  direction. The spin excitations correspond to in-plane modes  $\phi$  with an ellipsoidal shape elongated along  $y$  (cyclons) and out-of-plane modes  $\psi$  (extra-cyclons) with an ellipsoidal shape elongated along the tangent vector that belongs to the  $xz$  plane. **b**, Schematic of the experimental set-up used to apply an external electric field  $E$  to  $\text{BiFeO}_3$  single crystals and to probe its spin excitations using Raman spectroscopy. The electrodes are deposited on the  $(010)$  plane. A positive (negative) electric field parallel to the  $[010]$  ( $[0\bar{1}0]$ ) direction allows the orientation of the ferroelectric moment  $\mathbf{P}_1$  ( $\mathbf{P}_2$ ) along the  $[111]$  ( $[\bar{1}\bar{1}1]$ ) direction. Raman scattering is carried out through the ITO top electrode with light polarizations in the  $(010)$  plane. **c**, Raman spectra showing the magnon modes  $\phi_2$ ,  $\psi_2$ ,  $\phi_3$ ,  $\psi_3$  and  $\phi_4$  when the applied field ranges from 0 to  $75 \text{ kV cm}^{-1}$ . The dashed lines are guides to the eye following the shifts in frequency of each mode.

3 and 4 leading to frequency shifts that are symmetric to the ones along 1 and 2. The  $\psi_2$  mode is also directly connected to the polarization loop, but exhibits an opposite behaviour with respect to the  $\phi_2$  mode (Fig. 2b). The extra-cyclon mode  $\psi_2$  presents a much stronger frequency shift under the effect of an electric field of  $50 \text{ kV cm}^{-1}$ ,  $\Delta\omega_{\psi_2} = (+2.1 \pm 0.1) \text{ cm}^{-1}$ . Remarkably, the  $\psi_2$  frequency is seen to increase by over  $5 \text{ cm}^{-1}$  at maximum  $E$  field, corresponding to a 30% shift of its natural frequency. This experiment clearly demonstrates the coupling between the spin waves and the ferroelectric character of the material and that a spin-wave frequency hysteresis loop can be created and controlled at room temperature using the ferroelectric hysteresis loop.

There exist other methods for electric-field control of spin waves. A shift of the order of  $3 \times 10^{-5} \text{ cm}^{-1}$  (relative shift of 0.01%) has been detected in lithium ferrite under the application of similar voltages<sup>22</sup>. Recently, a Doppler shift of the order of  $10^{-3} \text{ cm}^{-1}$  (0.3%) has been demonstrated using electric currents<sup>23</sup>. The present experiment shows that the coupling between magnetic and ferroelectric degrees of freedom provides a much more efficient method for electric-field control of spin waves, with frequency shifts over  $5 \text{ cm}^{-1}$  (30%), several orders of magnitude larger than with previous methods.

The strong spin-wave frequency shifts that we observe may be interpreted as resulting from a combination of magnetoelectric interactions. The component of  $\mathbf{E}$  along  $\mathbf{P}$  (denoted  $E_z$ ) cannot play any role because of the competition with the internal electric

field parallel to  $\hat{z}$  produced by  $\mathbf{P}$ . Hence, we consider only interactions involving  $E_{\perp} = (E_x, E_y)$ . The Dzyaloshinskii–Moriya interaction that couples  $\mathbf{E}$  to  $\mathbf{M} \times \mathbf{L}$  is allowed by the  $R3c$  crystal symmetry of BFO (ref. 24), and also induces a transition from the cycloidal to a homogeneous spin state at large  $E_{\perp}$  (ref. 25). The Dzyaloshinskii–Moriya interaction produces spin-wave shifts that are independent of  $E$  at low electric field, at odds with the data, and that scale as  $E_{\perp}^2$  at larger field<sup>26</sup>. Another class of magnetoelectric interactions, the so-called flexoelectric interactions<sup>25,27</sup>, couple  $\mathbf{E}$  to gradients of  $\mathbf{L}$ . For example, the flexoelectric interaction in a homogeneous magnet leads to an instability towards a spiral state and to spin-wave shifts linear in  $E_{\perp}$  (ref. 27). However, in our case of bulk BFO the magnetic order is a cycloid that is itself induced by terms that couple  $\mathbf{P}$  to gradients of  $\mathbf{L}$  and have the same form as the flexoelectric interaction<sup>25,28</sup>. Therefore, there is a competition between these different couplings that leads to a renormalization of the cycloid wave vector. As both  $\omega_{\phi}$  and  $\omega_{\psi}$  are directly proportional to the cycloid wave vector, a large  $E_{\perp}$  will increase all spin-wave frequencies by the same amount. Thus, the Dzyaloshinskii–Moriya and the flexoelectric interactions are not able to reproduce the experimental data at lower field but might play a role at larger field.

Here, we have found that the spin-wave frequency shifts can be interpreted using the Landau free-energy model based on an additional kind of magnetoelectric interactions induced by the external electric field. Indeed, the  $R3c$  symmetry of BFO allows the

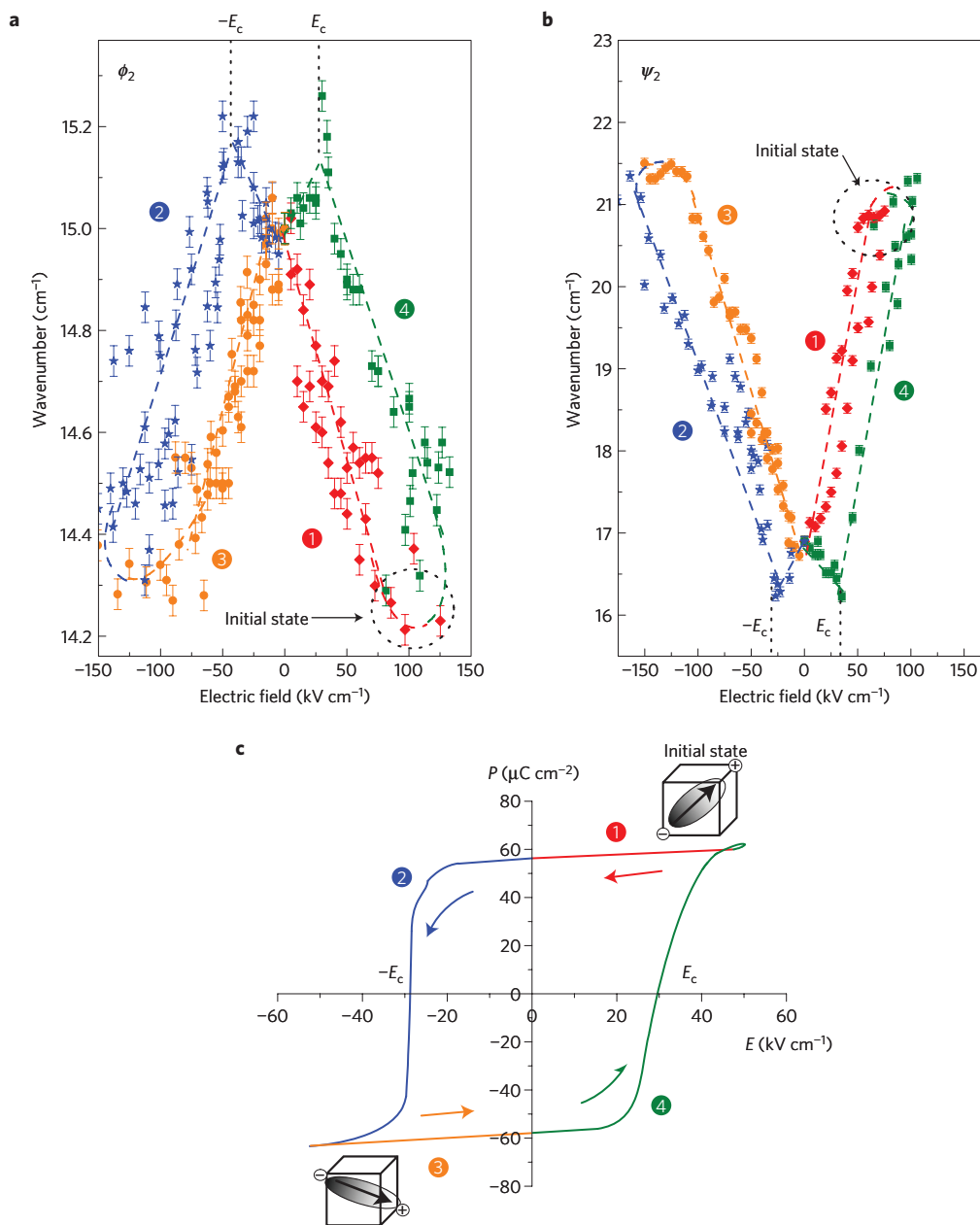


**Figure 2 | Spin-wave hysteresis loop.** **a,b**, Voltage dependence of  $\phi_2$  (**a**) and  $\psi_2$  (**b**) magnon modes. **c**, ( $P$ - $E$ ) hysteresis loop at room temperature. The shift of the spin-wave frequencies follows the polarization loop along 1 (red diamond), 2 (blue star), 3 (orange circle) and 4 (green square). The error was calculated for each point using the standard deviation of the individual peak location.

presence of two linear magnetoelectric interactions that couple the Néel order parameter  $\mathbf{L}$  directly with  $E_{\perp}$ ,

$$F_1 = \frac{1}{2} \kappa_1 E_{\perp} \cdot \mathbf{L}_{\perp} L_z \quad (1)$$

$$F_2 = \frac{1}{2} \kappa_2 E_{\perp} \cdot [(L_y^2 - L_x^2) \hat{x} + 2L_x L_y \hat{y}] \quad (2)$$

where  $\kappa_1$  and  $\kappa_2$  are phenomenological coupling constants. Physically,  $F_1$  and  $F_2$  model additional magnetic anisotropy energies induced by  $E_{\perp}$ . Hence their microscopic origin is related to spin-orbit coupling. The first interaction ( $F_1$ ) produces a redshift for both  $\psi_n$  and  $\phi_n$  modes when  $E_{\perp}$  is increased. Thus,  $F_1$  cannot explain the experimental observations at low  $E_{\perp}$  (Fig. 2a,b). On the other hand, the interaction  $F_2$  induces a blueshift for all  $\psi_n$  modes, and a redshift for  $\phi_n$  modes with  $n \geq 2$  as found experimentally (see Fig. 3). This interaction drives the system into a homogeneous

state when  $E_{\perp}$  becomes greater than a homogeneous critical field  $E_{hs} \propto 1/\kappa_2$ . The calculated curves show that cyclon and extra-cyclon mode frequencies converge to two fixed points at the critical field  $E_{hs}$ . A comparison between theory and experiment (Fig. 3) gives an estimate of  $E_{hs} \approx 160 \text{ kV cm}^{-1}$  (above the maximum electric field of  $125 \text{ kV cm}^{-1}$  that could be applied to our sample without damage). Calculations are in good agreement with the experimental data in the low-field region (see Fig. 3), but a clear deviation occurs at high fields. Interestingly, cyclon and extra-cyclon modes seem to merge for  $E > 0.5E_{hs}$ . This effect and the difference between theory and experiment at high fields might be due to other magnetoelectric interactions such as the Dzyaloshinskii–Moriya and the flexoelectric interactions discussed above.

The demonstration of electrical control of spin-wave states represents a significant step towards making new spin-wave-based technologies. The cyclon spin-wave dispersion can be

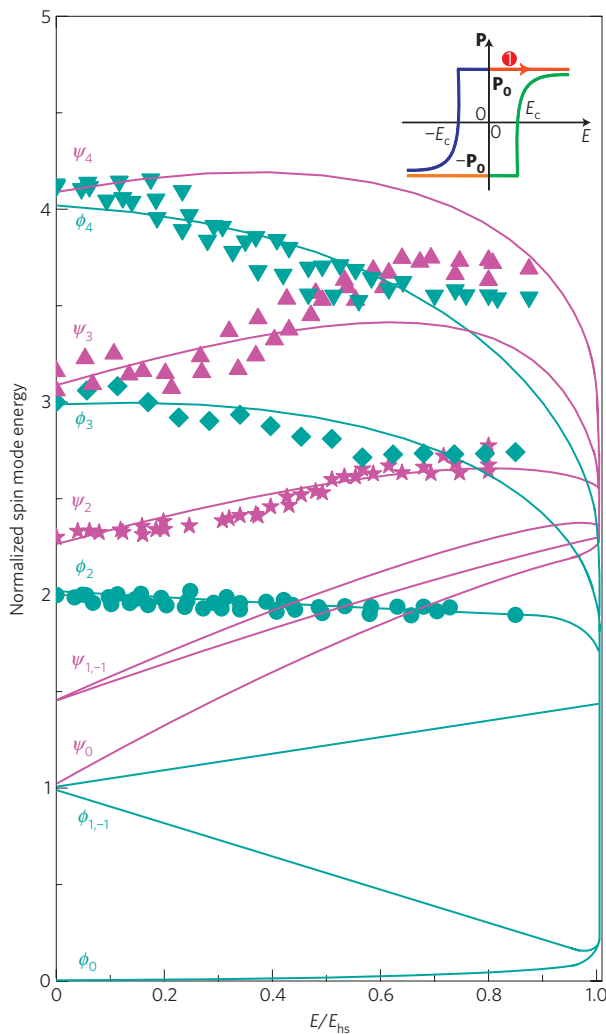


**Figure 3 | Electric-field dependence of the measured and calculated spin-wave frequencies.** When the applied electric field is zero, the energies of the  $\phi_n$  and  $\psi_n$  modes are  $E_{\phi_n} = n v_0 Q$  and  $E_{\psi_n} = \sqrt{1+n^2} v_0 Q$  respectively, with index  $n$  labelling the modes,  $v_0 = 1.4 \times 10^6 \text{ cm s}^{-1}$  being the fundamental cyclon spin-wave velocity and  $Q$  being the cycloid wave vector<sup>10</sup>. The figure shows the spin-wave mode energies normalized to  $v_0 Q$  as a function of the ratio of the applied electric field  $E$  divided by the electric field  $E_{hs}$  required to destroy the cycloid. When  $E > E_{hs}$  the spin ground state becomes homogeneous in space. The filled symbols are the experimental data obtained following path 1 (inset) in the polarization cycle using  $E \parallel [010]$  from 0 to  $125 \text{ kV cm}^{-1}$ :  $\phi_2$  (circle),  $\phi_3$  (diamond),  $\phi_4$  (down triangle),  $\psi_2$  (star),  $\psi_3$  (up triangle).  $\mathbf{P}$  is parallel to the  $[111]$  direction and no polarization flop occurs. The solid lines are explicit numerical calculations obtained from a dynamical Ginzburg–Landau theory based on the linear magnetoelectric interaction  $F_2$ .

written as  $\omega_\phi = v_\phi k$ , and the extra-cyclon dispersion as  $\omega_\psi = v_\psi \sqrt{k^2 + Q^2}$ . For  $E = 0$ , the spin-wave velocities are equal,  $v_\phi = v_\psi = v_0 = 1.4 \times 10^6 \text{ cm s}^{-1}$  (ref. 10). However, under an electric field of  $100 \text{ kV cm}^{-1}$  the  $\phi$  and  $\psi$  spin-wave velocities are tuned by  $\Delta v_\phi = -6 \times 10^4 \text{ cm s}^{-1}$  and  $\Delta v_\psi = +4 \times 10^5 \text{ cm s}^{-1}$ , respectively. Whereas the speed of electron spin precession in a magnetic field is generally fixed by intrinsic properties of the materials considered, our work shows that in a multiferroic the spin-wave speed can be continuously adjusted and in a different way depending on the spin propagating mode by the applied electric fields.

We have demonstrated that the frequency of spin waves can be tuned electrically by over 30% at room temperature

in multiferroic  $\text{BiFeO}_3$ . This electric-field dependence mimics that of the ferroelectric polarization, providing a handle for the non-volatile, low-power control of spin waves. Thus, aside from its potential for spintronics<sup>29</sup> and photonics<sup>30</sup>,  $\text{BiFeO}_3$  emerges as an exciting platform for testing new magnonic device concepts, which further confirms it as a key multifunctional material for technologies beyond complementary metal–oxide–semiconductors.

## Methods

**Experimental details.**  $\text{BiFeO}_3$  single crystals were grown in air using  $\text{Bi}_2\text{O}_3$ – $\text{Fe}_2\text{O}_3$  flux in an alumina crucible as detailed in ref. 12. Polarized optical microscope images of the samples show that the crystal consists of one single ferroelectric domain<sup>12</sup>. Neutron measurements on the same samples have shown the presence of one antiferromagnetic domain<sup>16</sup>. A conducting indium tin oxide (ITO) layer was grown by pulsed laser deposition on the top of the (010) sample surface to apply a uniform electric field. ITO has no Raman signal in the frequency range of interest. All of the measurements were carried out in vacuum at room temperature on several samples.

Raman scattering was carried out on the (010) sample surface in the backscattering geometry using the 647.1 nm laser line. Raman scattering is collected by a triple spectrometer Jobin Yvon T64000 equipped with a CCD (charge-coupled device). The spot size is about  $100 \mu\text{m}^2$  and the penetration depth is less than  $10^{-5} \text{ cm}$ . Reproducible Raman measurements have been carried out on several points on the sample surfaces.

The  $\phi_n$  and  $\psi_n$  modes ( $n$  index labels the modes from their lowest to highest energy) were selectively observed using parallel and crossed polarizations in the (010) plane, respectively (see Supplementary Information). The polarizations are defined with respect to the projection of the cycloid wave vector  $Q \parallel [10\bar{1}]$  in the (010) plane (the direction of the wave vector  $Q$  is not directly accessible in the (010) plane). To show simultaneously several  $\phi_n$  and  $\psi_n$  modes, the figures in the Supplementary Information present measurements without specific polarization.

**Theoretical method.** We consider a total free energy given by  $F = F_0 + F_1 + F_2$ , with  $F_0$  being the usual model free energy of multiferroic BFO (ref. 21,25),

$$F_0 = \frac{A}{2} L^2 + \frac{r}{2} M^2 + \frac{G}{4} L^4 + \frac{c}{2} \sum_{i=x,y,z} (\nabla L_i)^2 - \alpha_p \mathbf{P} \cdot [\mathbf{L}(\nabla \cdot \mathbf{L}) + \mathbf{L} \times (\nabla \times \mathbf{L})] \quad (3)$$

and  $F_1, F_2$  given by equations (1) and (2) respectively (we omit the purely ferroelectric contributions to equation (3) because they play no role in the discussion below). Here  $A, r, G, c$  and  $\alpha_p$  are phenomenological constants. The ground state is determined by the condition  $\delta F / \delta \mathbf{L} = 0$ ; when  $E_\perp = 0$  the ground state is a harmonic cycloid  $\mathbf{L}_0 = L_0 [\sin(Qx)\hat{x} + \cos(Qx)\hat{z}]$  with wave vector  $Q = \alpha_p / c$  and amplitude  $L_0^2 = (-A + cQ^2) / G$ . The effect of  $E_\perp$  is to reduce the ground-state wave vector  $Q$  and to add additional anharmonic contributions to  $\mathbf{L}_0$  at odd multiples of  $Q$ . When  $E_\perp$  is equal to a critical field  $E_{hs} = ((\pi \alpha_p P)^2 / 4c) / (1/\kappa_2)$ , the cycloid wave vector  $Q$  becomes equal to zero, signalling a transition to a homogeneous state.

The spin-wave excitation frequencies are determined from the Landau–Lifshitz equations of motion. After combining the equations of motion for the order parameters  $\mathbf{L}$  and  $\mathbf{M}$  we get

$$\frac{\partial^2 \mathbf{L}}{\partial t^2} = -r(\gamma L_0)^2 \left[ \frac{\delta F}{\delta \mathbf{L}} - \left( \dot{\mathbf{L}}_0 \cdot \frac{\delta F}{\delta \mathbf{L}} \dot{\mathbf{L}}_0 \right) \right] \quad (4)$$

where  $\gamma$  is the gyromagnetic ratio. We find wave-like solutions by plugging in  $\mathbf{L} = \mathbf{L}_0 + (\delta \mathbf{L}) e^{i\omega t}$  in equation (4), with  $(\delta \mathbf{L}) = \phi(x)\hat{\mathbf{D}} + \psi(x)\hat{\mathbf{y}}$ . The unitary vector  $\hat{\mathbf{D}}$  is tangential to  $\mathbf{L}_0$ ; that is, it is orthogonal to  $\mathbf{L}_0$  but lies within the cycloid plane. Plugging  $\phi(x) = \sum_n \phi_n e^{inQx}$ , and  $\psi(x) = \sum_n \psi_n e^{imQx}$ , into equation (4) leads to a matrix equation with eigenvalues that give the spin-wave excitations at  $k = 0$ .

We underline that the free-energy model for BFO equation (3) does not contain any magnetic anisotropy. Nevertheless, the present experiment shows that an external  $E$  field induces magnetic anisotropy linear in  $E$  (see equation (2)). In other words, the electric field activates a latent anisotropy in the material, leading to a large effect in the case of equation (2).

Received 3 August 2010; accepted 12 October 2010; published online 14 November 2010

## References

- Kruglyak, V. V., Demokritov, S. O. & Grundler, D. Magnonics. *J. Phys. D* **43**, 264001 (2010).
- Kajiwar, Y. *et al.* Transmission of electrical signals by spin-wave interconversion in a magnetic insulator. *Nature* **464**, 262–267 (2010).

- Khitun, A., Bao, M. & Wang, K. L. Magnonic logic circuits. *J. Phys. D* **43**, 264005 (2010).
- Schneider, T. *et al.* Realization of spin-wave logic gates. *Appl. Phys. Lett.* **92**, 022505 (2008).
- Catalan, G. & Scott, J. F. Physics and applications of bismuth ferrite. *Adv. Mater.* **21**, 2463–2485 (2009).
- Eerenstein, W., Mathur, N. D. & Scott, J. F. Multiferroic and magnetoelectric materials. *Nature* **442**, 759–765 (2006).
- Chu, Y.-H. *et al.* Electric-field control of ferromagnetism using a magnetoelectric multiferroic. *Nature Mater.* **7**, 478–482 (2008).
- Chappert, C., Fert, A. & Nguyen Van Dau, F. The emergence of spin electronics in data storage. *Nature Mater.* **6**, 813–823 (2007).
- Pimenov, A., Mukhin, A. A., Ivanov, V. Y., Balbashov, A. M. & Loidl, A. Possible evidence for electromagnons in multiferroic manganites. *Nature Phys.* **2**, 97–100 (2006).
- Cazayous, M. *et al.* Possible observation of cycloidal electromagnons in BiFeO<sub>3</sub>. *Phys. Rev. Lett.* **101**, 037601 (2008).
- Pimenov, A., Shuvaev, A. M., Mukhin, A. A. & Loidl, A. Electromagnons in multiferroic manganites. *J. Phys. Condens. Matter* **20**, 434209 (2008).
- Lebeugle, D. *et al.* Room-temperature coexistence of large electric polarization and magnetic order in BiFeO<sub>3</sub> single crystals. *Phys. Rev. B* **76**, 024116 (2007).
- Smolenski, G. A., Yudin, V. M., Sher, E. S. N. & Stolypin, Y. E. Antiferromagnetic properties of some perovskites. *Sov. Phys. JETP* **16**, 622–624 (1963).
- Lee, S. *et al.* Single ferroelectric and chiral magnetic domain of single-crystalline BiFeO<sub>3</sub> in an electric field. *Phys. Rev. B* **78**, 100101(R) (2008).
- Sosnowska, I., Peterlin-Neumaier, T. & Steichele, E. Spiral magnetic ordering in bismuth ferrite. *J. Phys. C* **15**, 4835–4846 (1982).
- Lebeugle, D. *et al.* Electric-field-induced spin flop in BiFeO<sub>3</sub> single crystal at room temperature. *Phys. Rev. Lett.* **100**, 227602 (2008).
- Zhao, T. *et al.* Electrical control of antiferromagnetic domains in multiferroic BiFeO<sub>3</sub> films at room temperature. *Nature Mater.* **5**, 823–829 (2006).
- Baek, S. H. *et al.* Ferroelastic switching for nanoscale non-volatile magnetoelectric devices. *Nature Mater.* **9**, 309–314 (2010).
- Singh, M. K., Katiyar, R. & Scott, J. F. New magnetic phase transitions in BiFeO<sub>3</sub>. *J. Phys. Condens. Matter* **20**, 252203 (2008).
- Rovillain, P. *et al.* Polar phonons and spin excitations coupling in multiferroic BiFeO<sub>3</sub> crystals. *Phys. Rev. B* **79**, 180411(R) (2009).
- de Sousa, R. & Moore, J. E. Optical coupling to spin waves in the cycloidal multiferroic BiFeO<sub>3</sub>. *Phys. Rev. B* **77**, 012406 (2008).
- Rado, G. T., Vittoria, C., Ferrari, J. M. & Remeika, J. P. Linear electric field shift of a ferromagnetic resonance: Lithium ferrite. *Phys. Rev. Lett.* **41**, 1253–1255 (1978).
- Vlaminck, V. & Bailleul, M. Current-induced spin-wave Doppler shift. *Science* **322**, 410–413 (2008).
- de Sousa, R. & Moore, J. E. Comment on ‘Ferroelectrically induced weak ferromagnetism by design’. *Phys. Rev. Lett.* **102**, 249701 (2009).
- Sparavigna, A., Strigazzi, A. & Zvezdin, A. Electric-field effect on the spin-density wave in magnetic ferroelectrics. *Phys. Rev. B* **50**, 2953–2957 (1994).
- de Sousa, R. & Moore, J. E. Electrical control of magnon propagation in multiferroic BiFeO<sub>3</sub> films. *Appl. Phys. Lett.* **92**, 022514 (2008).
- Mills, D. L. & Dzyloshinskii, I. E. Influence of electric fields on spin waves in simple ferromagnets: Role of the flexoelectric interaction. *Phys. Rev. B* **78**, 184422 (2008).
- Zvezdin, A. K. & Pyatakov, A. P. Flexomagnetoelectric effect in bismuth ferrite. *Phys. Status Solidi B* **246**, 1956–1960 (2009).
- Béa, H., Gajek, M., Bibes, M. & Barthélémy, A. Spintronics with multiferroics. *J. Phys. Condens. Matter* **20**, 434221 (2008).
- Choi, T., Lee, S., Choi, Y. J., Kiryukhin, V. & Cheong, S.-W. Switchable ferroelectric diode and photovoltaic effect in BiFeO<sub>3</sub>. *Science* **324**, 63–66 (2009).

### Acknowledgements

The authors would like to thank R. Lobo and P. Monod for fruitful discussions and E. Jacquet for technical assistance. D.C., M.B. and A.B. would like to acknowledge support from the French Agence Nationale pour la Recherche, contract MELOIC (ANR-08-P196-36). R.d.S. would like to acknowledge support from the Natural Sciences and Engineering Research Council of Canada.

### Author contributions

The samples were grown by A.F. and D.C.; P.R., M.C., M.B. and A.B. designed the experiment; P.R. and M.C. carried out experiments and analysed data; R.d.S. developed the model and analysed data. All authors discussed the results and wrote the manuscript.

### Additional information

The authors declare no competing financial interests. Supplementary information accompanies this paper on [www.nature.com/naturematerials](http://www.nature.com/naturematerials). Reprints and permissions information is available online at <http://npg.nature.com/reprintsandpermissions>. Correspondence and requests for materials should be addressed to M.C.